Asociación Argentina
de Mecánica Computacional

Mecánica Computacional Vol XXXVII, págs. 33-42 (artículo completo)
A. Cardona, L. Garelli, J.M. Gimenez, P.A. Kler, S. Márquez Damián, M.A. Storti (Eds.)
Santa Fe, 5-7 Noviembre 2019

# TWO-WAY SHEAR STRENGTH OF REINFORCED CONCRETE SLAB-COLUMN CONNECTIONS: INFLUENCE OF TESTING CONDITIONS IN ISOLATED SPECIMENS

**Leandro S. Montagna**[a]

[a]*Ferguson Structural Engineering Laboratory, University of Texas at Austin, 110 Inner Campus Drive, 78705 Austin, Texas, Estados Unidos, fsel-main@austin.utexas.edu, http://fsel.engr.utexas.edu*

**Keywords:** Flat plate, punching shear, two-way shear.

**Abstract**. To assess the two way shear resistance, or punching shear strength, of reinforced concrete slabs, code provisions fitted from experimental data are typically employed. The experimental data forming the bases of these provisions have generally consisted of isolated slab column connection tests. This research is focused on exploring the variation in the punching performance of slab column connections when the typical testing conditions used to investigate isolated slab specimen are varied in a manner that produces alternative sectional loading conditions within the column connection region. Results are presented from an experimental program conducted at the Ferguson Structural Engineering Laboratory (FSEL) of The University of Texas at Austin and a comparison is presented with estimations made from numerical models. The data is used to scrutinize current design and analysis procedures, and to shed light on the significance of the sectional loading conditions in the light of flat plate connection shear resisting performance.

## 1 INTRODUCTION

The punching resistance, or the two-way shear strength, of flat slab or flat plate systems in the vicinities of the column-supported regions has been the focus of extensive investigation. This research has been largely motivated by the fact that punching failures involve typically brittle failure mechanisms and, as such, can propagate and cause partial, or even total, collapse of a structure (Hawkins and Mitchell 1979).

To experimentally assess the punching shear strength of RC flat plates, isolated slab elements loaded by way of some form of integrated column stub are commonly considered, see Figure 1. These specimens seek to represent the negative moment area comprising the slab-column connection region.

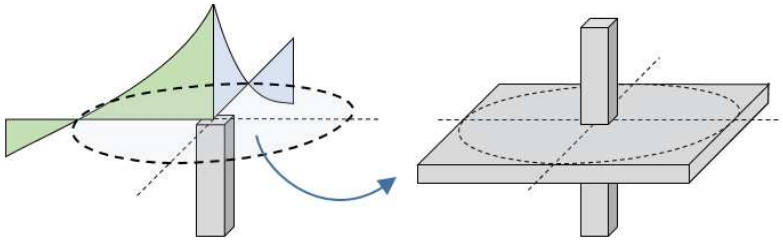

Figure 1: Negative moment region of the slab-column connection.

Phenomena such as moment redistribution and compressive membrane action do not occur in isolated specimens and are likely to increase the actual punching shear strength of RC flat plate systems (Einpaul et al. 2016; Goh and Hrynyk 2017). Thus, punching shear strength design provisions typically derived on the basis of data obtained from experiments done on isolated specimens, in general provide conservative estimations.

This research focuses on exploring the variation in the punching shear strength of RC slab-column connections when the applied loading is changed from concentrated loading conditions, which are typical to these types of tests, to the application of loads that are distributed over the slab surface, as illustrated in Figure 2. This change influences the combination of bending moment and out-of-plane shear applied to the slab-column connection.

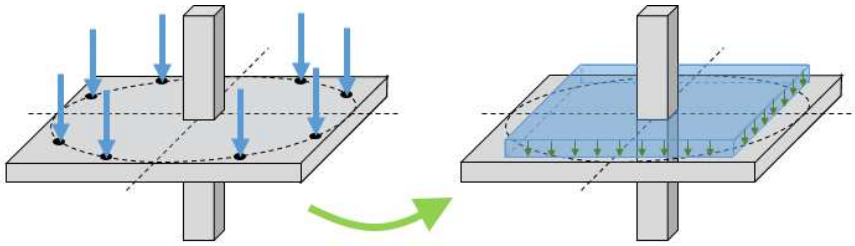

Figure 2: Concentrated loading conditions (left) and uniform pressure over the slab surface (right).

Additionally, the results obtained from the experiments are contrasted with shear strength estimates obtained from numerical models and applying the provisions from: i) ACI 318-14 (American Concrete Institute Committee 318 2014), ii) Eurocode 2 (European Committee for Standardization 2004), and other formulations such as iii) fib Model Code 2010 (International Federation for Structural Concrete 2010), and iv) Critical Shear Crack Theory (CSCT) (Muttoni 2008).

Finally, it should also be noted that the research presented is limited to the investigation of slab-column connections constructed without shear reinforcement.

## 2 EXPERIMENTAL PROGRAM

The experimental program was part of a larger testing program carried-out at the Ferguson Structural Engineering Laboratory of the University of Texas at Austin. Results from other stages of this program are presented in Glikman et al. (2017). The program consisted of four full-scale isolated RC slab-column connections, as summarized in Table 1. The test specimens were designed as two pairs of nominally-identical specimens.

| # | Slab designation | Hogging reinforcement ratio, $\rho_l$ (%) | Transverse reinforcement ratio, $\rho_v$ (%) | Testing method |
|---|---|---|---|---|
| 1 | C-1.0 | 1.00 | 0 | CL [(a)] |
| 2 | U-1.0 | 1.00 | 0 | UL [(b)] |
| 3 | C-0.7 | 0.72 | 0 | CL [(a)] |
| 4 | U-0.7 | 0.72 | 0 | UL [(b)] |
| (a) CL test setup,(b) UL test setup | | | | |

Table 1: Summary of the experimental program.

Current code formulations to evaluate punching shear strength are based on tests of isolated slab elements that are typically tested with loads being applied as concentrated forces along the line of moment contraflexure. This leads to acceptable, but potentially artificial estimations, of the punching shear resistance and makes the testing much simpler and cost-efficient. However, the way the load is applied to the specimens in these tests may be significantly different from real-world cases. Thus, the main purpose of the experimental program presented in this thesis was to examine how the punching shear strength was affected as a result of varied applied loading scenarios.

Two different testing approaches were used to fail the isolated slab-column connection specimens. Half of the specimens were tested using a setup with similar characteristics to those used by others in the past to assess punching shear strength of slab-column connections (Birkle & Dilger 2008, Guandalini et al 2009, Einpaul et al 2016). A vertical force was applied to the intersecting column while the slab was vertically-restrained using a series of rigid struts. In this document, the apparatus for this testing procedure is referred to as a Concentrated Load (CL) test setup and the main characteristics are displayed in Figure 3.

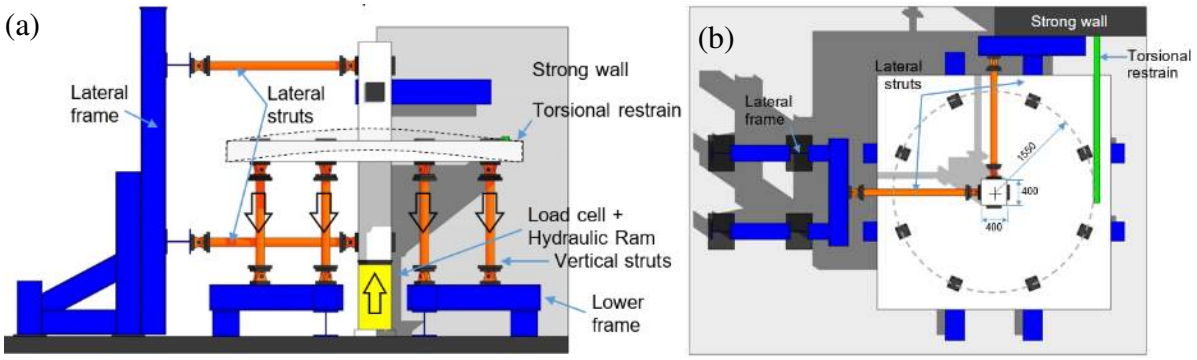


Figure 3: CL Test Setup: (a) front, (b) top view, dimensions (mm).

The other half of the testing specimens were loaded to failure using an innovative testing approach, designated in this thesis as the Uniform Load (UL) test setup. In the UL testing procedure, loads were applied by way of an increasing distributed surface pressure applied to

the slab using a series of airbags. The slab was restrained vertically using a high-strength rod that passed through the center-point of the specimen (i.e., through the column stub) and was fastened to a stiff reaction frame, see Figure 4.

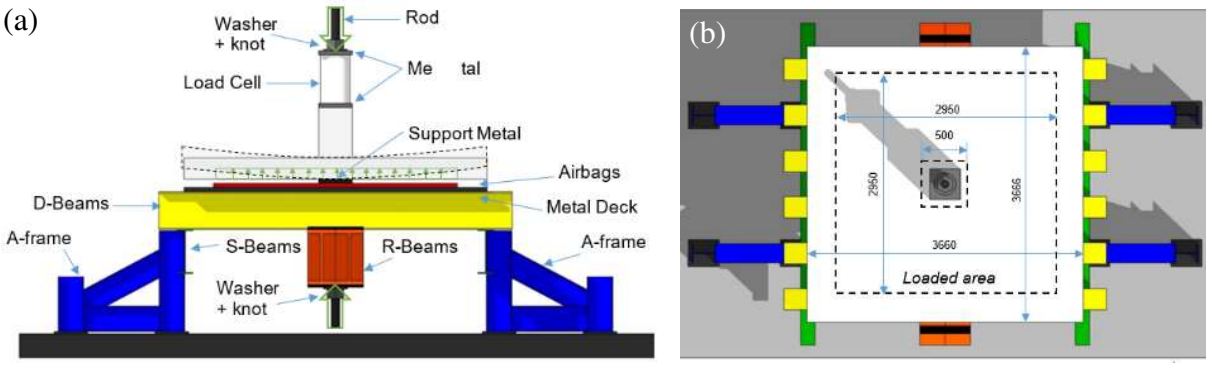


Figure 4: UL Test Setup: (a) front, (b) top view, dimensions (mm).

Key dimensions of the test specimens used in each testing configuration are shown in Figure 5. It should also be noted that different RC column configurations were used for the two slab testing procedures employed.

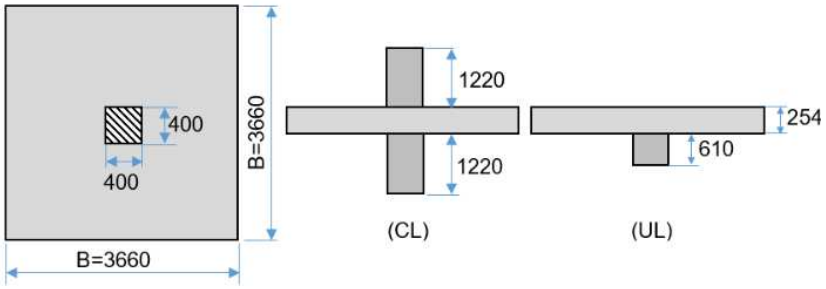


Figure 5: Main dimensions of specimens (mm). Left to right: Top view, lateral view of specimen for CL test setup, lateral view of specimen for UL test setup.

The edge boundaries of the slabs were free to rotate and translate laterally. Further, all of the slab-column connection assemblies were constructed without through-thickness slab shear reinforcement. In all cases, a lower and an upper orthogonal grid of longitudinal reinforcement was provided. US No. 6 steel reinforcing bars were provided for the top mat of longitudinal reinforcement, which served as the flexural tension reinforcement. US No. 3 steel reinforcing bars were used for bottom mat of reinforcement which was located near the compressive surface of the slab. Note that the primary difference amongst the test specimens was the amount of longitudinal reinforcement provided in the top layer (i.e., on the flexural tension side). A clear cover of 20 mm. was provided for all reinforcing bars comprising the slabs. Given the aforementioned construction details, the mean effective depth was 216 mm. and was the same for all four slab specimens (refer to Figure 6).

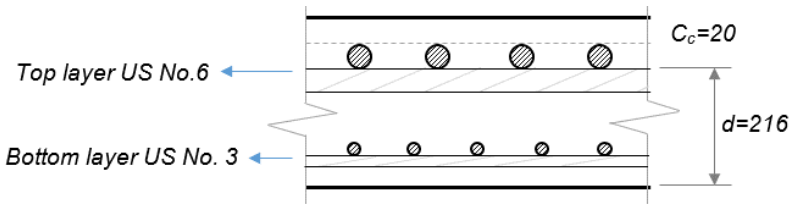


Figure 6: Mean effective depth (d) of both orthogonal directions of hogging reinforcement of the specimens.

The negative, or hogging, reinforcement ratio ($\rho_l$) of the slab was defined as the amount of flexural tension reinforcement placed in the top layer (in one of the two orthogonal directions) divided by the effective area of the slab $B \cdot d$:

$$\rho_l[\%] = \frac{A_s}{B \cdot d} \cdot 100 \quad (1)$$

Where, $A_s$ is the nominal area of reinforcing steel, $d$ is the mean effective depth and $B$ is the width of the slab.

Additionally to the measurement of the applied load onto the specimen, instrumentation was provided in order to record deflections and reinforcing bar strains. Linear potentiometers, or LPOTs, were installed to record deflections at several points along the four directions of fabrication (N, S, W and E) of the specimens and strain gauges were installed at several locations on the longitudinal steel reinforcing bars for the purpose of measuring strains.

## 2.1 Material properties

Key mechanical properties for the concrete used in the construction of each specimen are shown in the Table 2.

| # | **Designation:** | **Age** [days] | $f_c'$ (a) (MPa) | $f_{ct}$ (b) (MPa) | $f_r$ (c) (MPa) | $f_t'$ (d) (MPa) |
|---|---|---|---|---|---|---|
| 1 | C-1.0 | 87 | 29.58 | 4.38 | 4.81 | 2.35 |
| 2 | U-1.0 | 48 | 34.41 | 5.38 | 4.56 | 2.96 |
| 3 | C-0.7 | 51 | 42.54 | 5.21 | 4.14 | 2.72 |
| 4 | U-0.7 | 56 | 43.02 | 4.48 | 5.03 | 2.96 |
| (a) Compressive Strength Test (ASTM C39), (b) Split Tension Test (ASTM C496), (c) Modulus of Rupture Test (ASTM C78), (d) Direct Tension Test (No standard) | | | | | | |

Table 2: Main properties of concrete in each specimen

The main material parameters evaluated for the steel reinforcement employed in this testing program are shown in Table 3.

| Size | Diameter (mm) | Area ($mm^2$) | $F_Y$ (MPa) | $F_u$ (MPa) | $E_S$ (MPa) | $\varepsilon_{sh}$ ($x10^{-3}$) | $\varepsilon_u$ ($x10^{-3}$) |
|---|---|---|---|---|---|---|---|
| US No. 3 | 9.53 | 71 | 441 | 669 | 199,060 | 7 | 100 |
| US No. 6 | 19.05 | 284 | 462 | 745 | 186,630 | 7 | 100 |

Table 3: Main properties of steel bars for all specimens.

## 2.2 Comparison between experiments

The normalized shear resistance $V_n/\left(\sqrt{f_c'}db_0\right)$ is plotted against the rotation $\psi$ for all specimens in Figure 7. From the plot it is possible to observe that tests conducted in the CL apparatus reached consistently lower punching shear resistances and developed much greater rotations for all normalized shear load levels when compared with the data obtained from the tests conducted on the UL apparatus.

Formulations to estimate punching shear strength considered in this document are fitted from experiments performed using testing procedures that have typically been similar in concept to the Concentrated Load test setup used to test specimens C-1.0 and C-0.7 of the

experimental program. Given the findings in Figure 7, is arguable if having a static/constant procedure for all loading scenarios is rational. Moreover, in real-world cases, depending on the structure, one test setup may be more representative than the other.

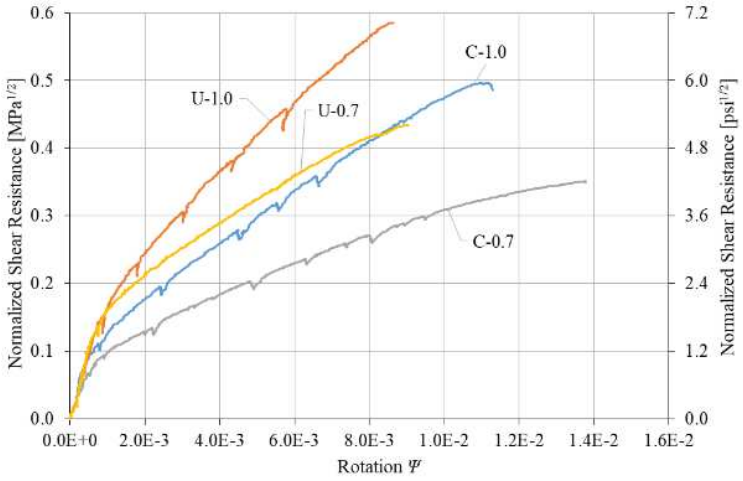


Figure 7: Comparison between tests. Normalized shear resistance vs Rotation

The North-American building code provisions, ACI 318-14, do not account for the longitudinal steel reinforcement ratio $\rho_l$ to assess the punching shear resistance of slab-column connections, however, Eurocode 2 and *fib* Model Code 2010 do. As is possible to observe from the results presented in Figure 7, the approach taken by the American standard is not capable of capturing the trend clearly shown in the test data pertaining to the increase in punching resistance as a result of increased longitudinal steel reinforcement ratio. This observation has been made by many others in the past (Guandalini and Muttoni et al. 2009); however, all of these prior testing programs employed more conventional concentrated load testing procedures. Thus, it is interesting to note that this well-established trend was observed in both loading scenarios and, as such, was found to be independent of the loading condition employed in the test.

## 3 NUMERICAL SIMULATIONS

The numerical models were built to represent the specimens comprising the experimental program and the analyses were carried out to compare the results, assert the validity of the computer simulation as a good representation of the reality and extend the analyses to other cases. *VecTor4*, a nonlinear finite element analysis program was employed.

### 3.1 Material models

The models specified into the program to describe the behavior of the RC in the slab-column connections are listed in Table 4.

| | | | | |
|---|---|---|---|---|
| *Compression* | *Base Curve:* | Hognestad | *Steel Hysteresis:* | Seckin |
| | *Post-Peak:* | Park-Kent | *Rebar Dowel Action:* | Tassios |
| | *Softening:* | Vecchio 1992-A | *Rebar Buckling:* | Dhakal-Maekawa |
| *Tension Stiffening:* | | Modified Bentz | *Crack Spacing:* | CEB-FIP 1978 |
| *Tension Softening:* | | Bilinear | *Slip Distortion:* | Walraven |
| *Confinement:* | | Kupfer/Richart | Among others | |

Table 4: Models describing the mechanical behavior of RC

More information about material models and their implementation within the VecTor analysis software can be found elsewhere (Wong, Vecchio, and Trommels 2013).

### 3.2 Models characteristics

For each specimen, a quarter-slab model, see Figure 8, was considered and restraints were provided along the edges of the model to enforce symmetry conditions. The quarter-slab modeling approach was done to reduce computation times required for the analyses.

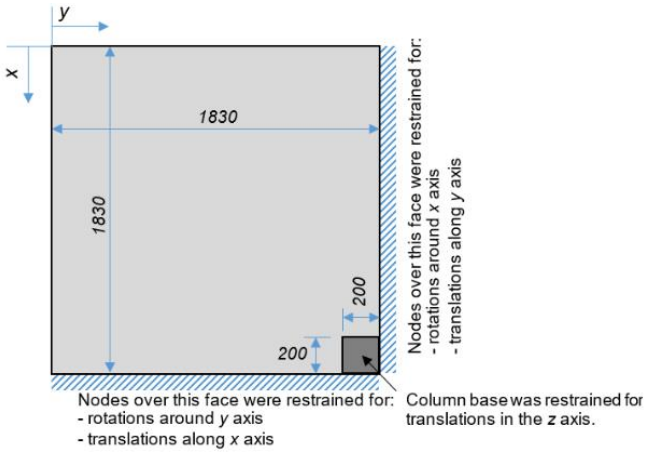


Figure 8: Dimensions and restraint conditions for the numerical models (mm)

The steel reinforcing bars used in the construction of the slabs was modeled discretely, using truss bar finite elements. Two types of steel reinforcement materials were specified for the truss elements, corresponding to US No. 3 and No. 6 reinforcing bars with mechanical properties provided in Table 3. The tension mat of reinforcement was modeled using the exact effective depths of the reinforcing bars provided in the *x* and *y* directions of the slab. However, the compressive mat of reinforcement was placed as a grid at the mean value of the (flexural) effective depth for the x and y directions.

Concrete materials used in the models had the same mechanical properties, listed in Table 2 for each specimen.

A common meshing strategy was used to model the slab regions for all analyses performed. The slab was divided into 10 linear brick finite elements through the depth and a brick element aspect ratio of approximately 1.0. This element sizing required 72 brick elements in each orthogonal direction and resulted in the use of 51,840 solid elements to represent the slab regions of the testing specimens. The models, as visualized in the input program, are displayed in Figure 9.

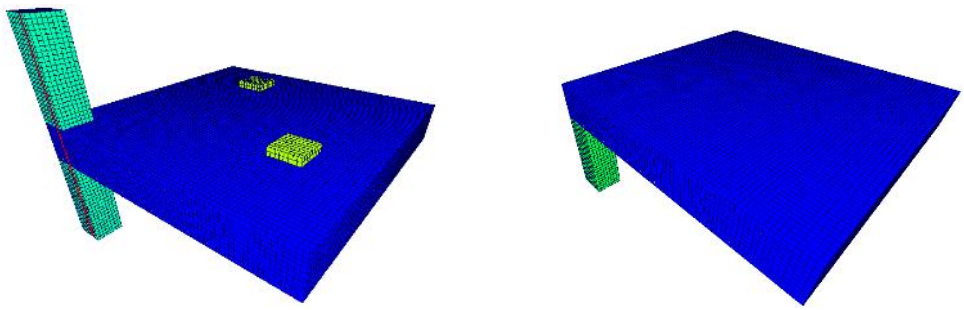

Figure 9: Model for CL specimens (left) and UL specimens (right).

The model was configured to simulate the conditions employed in the two different testing scenarios. In CL specimens, two rigid plates were added to the model at the locations restrained by the vertical support struts. At these locations prescribed vertical displacements were applied and the plate serves to distribute forces and avoid local punching failures from developing. In UL specimens, point load were applied to all the nodes inside the loaded area.

### 3.3 Comparison between Experiments and Numerical models

The normalized shear resistance $V_n/\left(\sqrt{f_c'}db_0\right)$ versus rotation $\psi$ response obtained from all numerical models and tests is presented in Figure 10.

The numerical models for the CL specimens, C-1.0 and C-0.7, reasonably captured the measured experimental responses. While typically overestimating slab stiffness, particularly in the initial cracking phase of the response, the shear resistances and the rotations of the slabs at failure are estimated with levels of accuracy that can typically be deemed suitable for slabs exhibiting brittle shear-controlled behaviors. Discrepancies in the response estimates may likely be attributed to the variability in the mechanical properties, specifically the tensile strength of concrete which plays an important role in the computation of post-cracking shear resisting response. The numerical models presented significant sensitivity to the variation of this parameter.

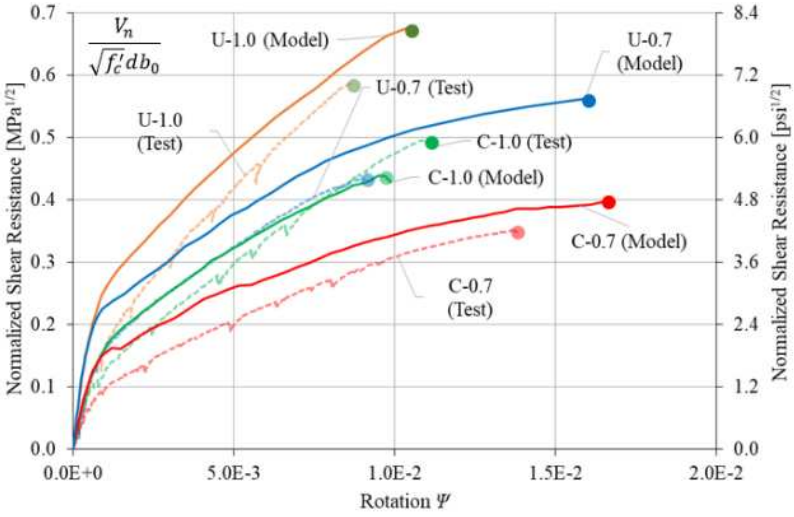


Figure 10: Normalized shear resistance $V_n/\left(\sqrt{f_c'}db_0\right)$ vs rotation ψ responses

The numerical models of UL specimens, U-1.0 and U-0.7, do not capture the experimental responses with the same degree of accuracy. The overall computed behaviors seem to be in-line with those measured; however, the tests failed at lower shear resistances than those estimated by way of numerical models.

When comparing the numerical model developed for a CL specimen with its nominally-identical counterpart tested on the UL apparatus (i.e. C-1.0 with U-1.0 and C-0.7 with U-0.7 respectively), it can be observed that failure occurs at around the same value of rotation, approximately 0.015 for models with hogging reinforcement ratios of 0.72 % and 0.011 for those with 1.00 %. However, as expected, models of UL specimens achieve higher failure loads due to the combination of bending moment and out-of-plane shear applied to the slab-column connection.

## 4 PUNCHING SHEAR STRENGTH FROM TESTS, NUMERICAL MODELS AND OTHER FORMULATIONS

The punching shear strength of the tested specimens is compared with the estimations from the numerical simulations and the formulations from ACI 318-14; Eurocode 2; *fib* Model Code 2010 and CSCT. The results are presented in Table 5. Note that all code-based shear strength estimates were done without the use of resistance or safety factors.

Both *fib* Model Code 2010 and CSCT were found to be the most accurate analytical models to predict punching shear strength consistently following the trends observed in the experimental data. CSCT provided the most accurate shear strength estimates; however, it did marginally over-predict the punching shear strength of specimens with low reinforcement ratios (by up to 7 % in the case of U-0.7). For the calculation of the punching shear strength by CSCT, the failure criterion is compared to a load-rotation response obtained from a non-linear elastic numerical model. This method is comparable to a *level of approximation IV* according to *fib* Model Code 2010 provisions. In the case other methods were used to determine the load-rotation response, i.e. yield line method, the punching shear resistance obtained would have been lower.

| SOURCE | SPECIMENS | | | | | | | | Avg. $V_n/V_t$ | *COV* |
|---|---|---|---|---|---|---|---|---|---|---|
| | ***C-1.0*** | | ***U-1.0*** | | ***C-0.7*** | | ***U-0.7*** | | | |
| | *(kN)* | $V_n/V_t$ | *(kN)* | $V_n/V_t$ | *(kN)* | $V_n/V_t$ | *kN* | $V_n/V_t$ | | |
| TEST | 1343 | - | 1708 | - | 1139 | - | 1415 | - | - | |
| Numerical | 1167 | 0.87 | 1934 | 1.13 | 1247 | 1.10 | 1776 | 1.25 | 1.09 | 0.15 |
| CSCT | 1182 | 0.88 | 1509 | 0.88 | 1194 | 1.05 | 1508 | 1.07 | 0.97 | 0.11 |
| *fib* 2010 | 968 | 0.72 | 1260 | 0.74 | 902 | 0.79 | 1192 | 0.84 | 0.77 | 0.07 |
| ACI 318 | 971 | 0.72 | 1047 | 0.61 | 1164 | 1.02 | 1171 | 0.83 | 0.80 | 0.22 |
| EC2 | 1025 | 0.76 | 1079 | 0.63 | 1035 | 0.91 | 1039 | 0.73 | 0.77 | 0.18 |

Table 5: Punching shear capacities obtained from tests, numerical simulations, and code/analysis procedures

Eurocode 2 was found to provide good estimates for shear strength capacity, especially considering the simplicity of the formulation. However, it is apparent that the Eurocode 2 procedure was unable to capture the influence of the different loading conditions developed in the test specimens comprising the experimental program (i.e., the influence of the different M/V ratios developed by way of the two test setups).

Lastly, ACI 318-14 mistakenly estimates that the punching shear strength will be larger for specimens with lower hogging reinforcement ratios leading towards unconservative shear strength estimates for the slab reinforced with 0.72 % flexural reinforcement. This result is reached given the difference in compressive strength of concrete between the specimens and by the fact that hogging reinforcement ratio is not accounted for.

The limitations of ACI 318-14 in its ability to accurately estimate punching shear strength of slab-column connections are at plain sight. Contrary to the trend observed in the tests, punching shear capacity increases with increasing reinforcement ratio, ACI 318 predicts the opposite: punching shear strength for the test specimens with low reinforcement ratios is greater. This inconsistency may actually produce designs with limited conservatism, as was the case for specimen C-0.7 (refer to Table 5). This starkly contrasts with findings made by others (Alexander and Hawkins 2005) who have indicated that the main asset of ACI 318 provisions was to foster safe and serviceable structures and not to produce accurate estimates of results from tests.

## 5 REFERENCES

American Concrete Institute. "ACI 318-14: Building Code Requirements for Structural Concrete and Commentary." (2008).

Alexander, S. D. B., and N. M. Hawkins. "A Design Perspective on Punching Shear." Special Publication 232 (2005): 97-108.

Birkle, Gerd, and Walter H. Dilger. "Influence of slab thickness on punching shear strength." *ACI Structural Journal* 105.2 (2008): 180.

Einpaul, Jürgen, Carlos E. Ospina, Miguel Fernández Ruiz, and Aurelio Muttoni. "Punching shear capacity of continuous slabs." *ACI Structural Journal* 113, no. 4 (2016): 861.

European Committee for Standardization. “Eurocode 2: Design of Concrete Structures”. (2004)

Glikman, Mario, Gabriel Polo, Oguzhan Bayrak, and Trevor D. Hrynyk. "Application of an Inclined Shear Reinforcing Assembly for Slab-Column Connections." *Special Publication*321 (2017): 7-1.

Goh, Chong Yik M., and Trevor D. Hrynyk. "Toward Practical Modelling of Reinforced Concrete Flat Slab Systems." IABSE Symposium Report. Vol. 109. No. 51. International Association for Bridge and Structural Engineering, 2017.

Guandalini, Stefano, Olivier L. Burdet, and Aurelio Muttoni. "Punching tests of slabs with low reinforcement ratios." ACI Structural Journal 106.1 (2009): 87.

Hawkins, Neil M., and Denis Mitchell. "Progressive collapse of flat plate structures." Journal Proceedings. Vol. 76. No. 7. 1979.

Code, Model. "Fib model code for concrete structures 2010." *Document Competence Center Siegmar Kästl eK, Germany* (2010).

Muttoni, Aurelio. "Punching shear strength of reinforced concrete slabs without transverse reinforcement." ACI structural Journal 105.EPFL-ARTICLE-116123 (2008)

Wong, P. S., F. J. Vecchio, and H. Trommels. "Vector2 & Formworks user’s manual second edition." (2013).